Synthesis and Characterization of Enantiomerically Pure *cis*- and *trans*-3-Fluoro-2,4-dioxa-8-aza-3-phosphadecalin 3-Oxides as γ-Homoacetylcholine Mimetics and Inhibitors of Acetylcholinesterase

by **Christian Clerc** and **Peter Rüedi***

Organisch-chemisches Institut der Universität Zürich,Winterthurerstrasse 190, CH-8057 Zürich (phone: +41 44 821 55 79; e-mail: peru@oci.uzh.ch)

The title compounds, the *P(3)*-axially and *P(3)*-equatorially substituted *cis*- and *trans*-configured 8-benzyl-3-fluoro-2,4-dioxa-8-aza-3-phosphadecalin 3-oxides (= 8-benzyl-3-fluoro-2,4-dioxa-8-aza-3-phosphabicyclo[4.4.0]decane 3-oxides = 2-fluorohexahydro-6-(phenylmethyl)-4*H*-1,3,2-dioxaphosphorino-[5,4-*c*]pyridine 2-oxides) were prepared (ee > 98%) and fully characterized (*Schemes 2* and *3*). The absolute configurations were established from that of their precursors, the enantiomerically pure *cis*- and *trans*-1-benzyl-4-hydroxypiperidine-3-methanols which were unambiguously assigned. Being configuratively fixed and conformationally constrained phosphorus analogues of acetyl γ-homocholine (= 3-(acetyloxy)-*N*,*N*,*N*-trimethylpropan-1-aminium), they are suitable probes for the investigation of molecular interactions with acetylcholinesterase. As determined by kinetic methods, all of the compounds are weak inhibitors of the enzyme.

1. Introduction. – In the preceding report [1], we have presented the synthesis and characterization of the optically active *P(3)*-axially and *P(3)*-equatorially substituted *cis*- and *trans*-configured 9-benzyl-3-fluoro-2,4-dioxa-9-aza-3-phosphadecalin 3-oxides of type **I** (*Scheme 1*). Continuing our investigations on the inhibition of serine hydrolases (chymotrypsin, acetylcholinesterase) by azadecalin-type organophosphates, we discuss now the preparation and full characterization of the eight stereoisomeric, enantiomerically pure 8-benzyl-3-fluoro-2,4-dioxa-8-aza-3-phosphadecalin 3-oxides (= 8-benzyl-3-fluoro-2,4-dioxa-8-aza-3-phosphabicyclo[4.4.0]decane 3-oxides = 2-fluorohexahydro-6-(phenylmethyl)-4*H*-1,3,2-dioxaphosphorino[5,4-*c*]pyridine 2-oxides) **10** and **11** representing type-**II** inhibitors (*cf. Schemes 1* and *3*) [2]. The compounds are mimetics of γ-homoacetylcholine (= 3-(acetyloxy)-*N*,*N*,*N*-trimethylpropan-1-aminium)[1]) and as such are considered to be suitable probes for the investigation of molecular interactions with acetylcholinesterase (AChE) [3][4] and the stereochemical course of the inhibition reaction by ^{31}P-NMR spectroscopy [5–7].

2. Synthesis and Characterization of the 3-Fluoro-2,4-dioxa-8-aza-3-phosphadecalins. – 2.1. *Precursor Diols* **2** *and* **3**. Following the protocol for the preparation of the

[1]) The trivial name 'γ-homoacetylcholine' is neither systematic nor is it common in the current literature. We have introduced this expression for the homologue of acetylcholine [3] and made use of it since then. Further common names used in the literature are acetyl homocholine and acetyl-γ-homocholine.

Scheme 1[a])

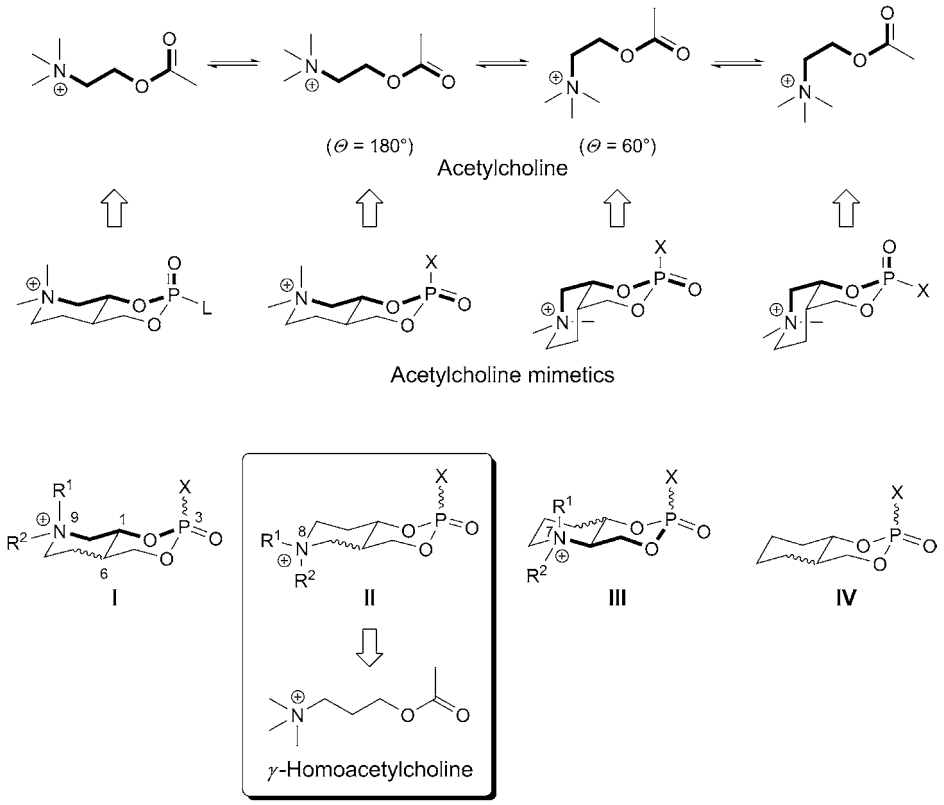

[a]) Structural types **I** – **IV**: *cis*- and *trans*-, and axially, and equatorially P-substituted isomers for each type
X = Selected electron-withdrawing group, *e.g.*, F, Cl, 4-nitrophenoxy, 2,4-dinitrophenoxy or amino acid derivatives (model compounds)
R^1, R^2 = (tert. amines, free bases) = H, Me, CH_2Ph; $R^1 = R^2$ or $R^1 \neq R^2$

racemic compounds [3], the optically active (+)- and (−)-*trans*-, and (+)- and (−)-*cis*-1-benzyl-3-(hydroxymethyl)piperidin-4-ols ((+)- and (−)-**2**, and (+)- and (−)-**3**, resp.) were obtained after reduction of ethyl 1-benzyl-4-oxopiperidine-3-carboxylate (**1**) with $NaBH_4$ and $LiAlH_4$ (*Scheme 2*). The resulting mixture (*ca.* 2:1) of the diols (±)-**2**/(±)-**3** was transformed *in situ* into the acetonides (±)-**4**/(±)-**5** that could easily be separated by column chromatography (SiO_2) into the pure *trans*- and *cis*-diastereoisomers (±)-**4** and (±)-**5**, respectively [3][8]. Preparative HPLC (*Chiralcel® OD*) of (±)-**4** afforded (+)-**4** ($[\alpha]_D = +29.2$, ee > 99%), and (−)-**4** ($[\alpha]_D = -28.7$, ee > 98%)[2]), and the

[2]) Although the method had been optimized ($R_S > 4$) [2], enantiomerically pure (−)-**4** ($[\alpha]_D = -29.3$, ee > 99%) could be obtained only in relatively small amounts, whereas bigger fractions of (−)-**4** did never exceed ee > 98%. As a consequence, the precursor (+)-**2** and the corresponding phosphadecalins (−)-**10a** and (−)-**10b** had only ee > 98% [2]. The $[\alpha]_D$ values were determined in acetone ($c = 1$).

analogous procedure with (±)-**5** gave (+)-**5** ($[\alpha]_D = +66.1$, ee > 99%), and (−)-**5** ($[\alpha]_D = -66.5$, ee > 99%). Hydrolysis of the acetonides yielded the *trans*- and *cis*-1-benzyl-3-(hydroxymethyl)piperidin-4-ols (+)-**2** ($[\alpha]_D = +9.2$, ee > 98%)[2]), (−)-**2** ($[\alpha]_D = -9.8$, ee > 99%), (+)-**3** ($[\alpha]_D = +16.7$, ee > 99%), and (−)-**3** ($[\alpha]_D = -16.6$, ee > 99%) (*Scheme 2*). As recently evidenced in detail [8], the absolute configurations were inferred by means of the high-field ^{1}H-NMR *Mosher* method [9] applied to the (*R*)- and (*S*)-MTPA ester couples **6a**/**6b**, **7a**/**7b**, **8a**/**8b**, and **9a**/**9b** (*Scheme 2*).

Scheme 2[2])

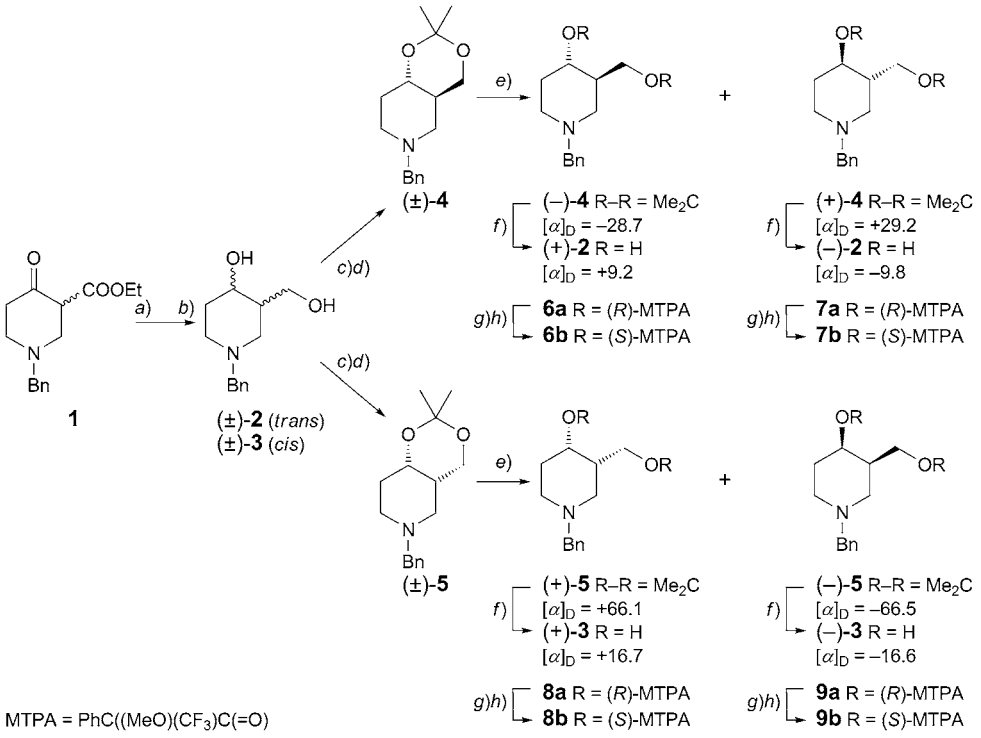

a) $NaBH_4$, Na_2CO_3, ^{i}PrOH, 10° (*cis*/*trans ca.* 1:2). *b*) $LiAlH_4$, Et_2O, r.t. *c*) $Me_2C(OMe)_2$, TsOH, CH_2Cl_2. *d*) CC (SiO_2, hexane/Et_2O) (steps *a*–*d* [3]). *e*) Prep. HPLC (*Chiralcel® OD*, hexane/EtOH). *f*) 1N HCl, 60°. *g*) (−)-(*R*)- or (+)-(*S*)-MTPA-Cl, resp., Et_3N, *N*,*N*-dimethylpyridin-4-amine (DMAP), CH_2Cl_2, r.t. (note: (*R*)-MTPA-Cl yields the (*S*)-MTPA-ester and *vice versa*). *h*) CC (SiO_2, AcOEt).

2.2. *3-Fluoro-2,4-dioxa-8-aza-3-phosphadecalins* **10** *and* **11**. Applying the established protocol [7], the *trans*-8-benzyl-3-fluoro-2,4-dioxa-8-aza-3-phosphadecalin 3-oxides **10** (*Scheme 3*) were prepared from (+)- or (−)-**2** by reaction with $POCl_2F$, and chromatographic separation of the resulting P(3)-epimer mixture (axial/equatorial *ca.* 1:1) gave the pure axial epimers (+)-**10a** (ee > 99%) and (−)-**10a** (ee > 98%)[2]) and the pure equatorial epimers (+)-**10b** (ee > 99%) and (−)-**10b** (ee > 98%)[2]). Similarly,

starting from (+)- or (−)-**3**, the *cis*-8-benzyl-3-fluoro-2,4-dioxa-8-aza-3-phosphadecalin 3-oxides (+)-**11a** and (−)-**11a**, and (+)-**11b** and (−)-**11b** were obtained (ee > 99%) (*Scheme 3*). However, because the *P(3)*-equatorially substituted congeners **10b** and **11b** had a pronounced tendency to epimerize, the chromatographic separation of the epimers was not as straightforward as for the type-**I** [1] and type-**IV** [10] compounds [2], see *Exper. Part*. Moreover, due to both facile epimerization at the P-atom and conformational changes of (+)- and (−)-**10b** and (+)- and (−)-**11b** [11][12] (see *Section 2.3*), the magnitude of the $[\alpha]_D$ values differed in the enantiomer pairs despite of equal ee (ee > 99% and ee > 98%, resp.)[2]).

Scheme 3[2])

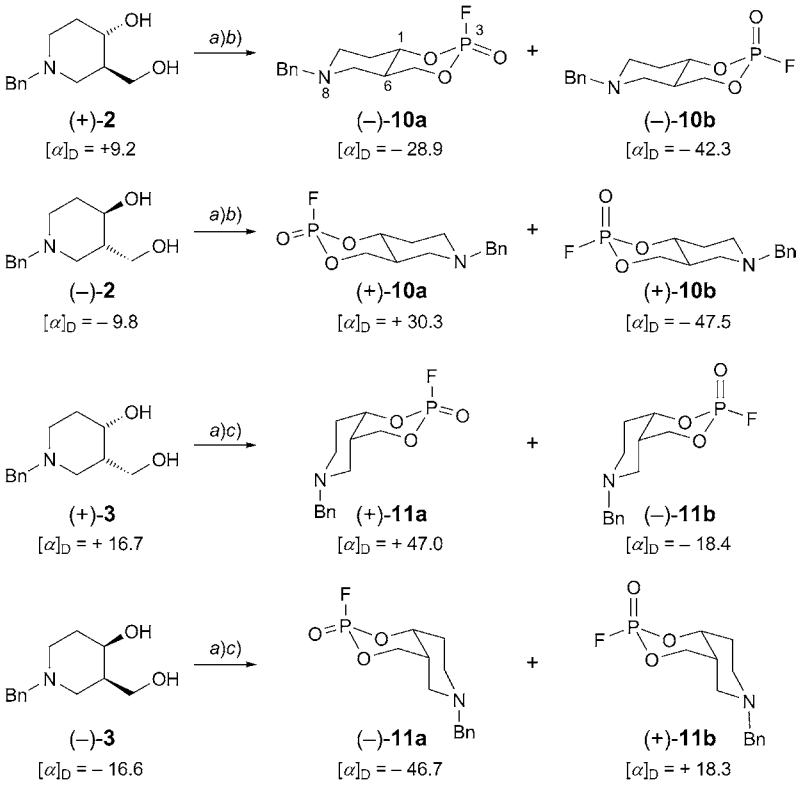

a) $P(O)Cl_2F$, pyridine, 0°. *b*) CC (SiO_2, Et_2O). *c*) CC (SiO_2, hexane/AcOEt/MeOH).

2.3. *Conformations of* **10** *and* **11** *in Solution.* The NMR data of the 2,4-dioxa-8-aza-3-phosphadecalins **10** and **11** (see *Exper. Part*) display the same essential features as the type-**I** [1] and type-**IV** [10] congeners (*Scheme 1*). They confirm the relative configuration at the P-atom, the double chair conformations of the axial epimers **10a** and **11a** and distorted conformations of the 2,4-dioxa-3-phospha moiety in the equatorial

epimers **10b** and **11b**[3]). Due to the strongly electronegative F-substituent, the chemical shift difference ($\Delta\delta = \delta_{eq} - \delta_{ax}$) is small in the *trans*-couple **10a**/**10b** ($\Delta\delta = +0.5$ ppm) and negative in the *cis*-couple **11a**/**11b** ($\Delta\delta = -0.4$ ppm) as discussed earlier [3][11].

As previously presented [1][3][5][6] and directly evidenced [11], the anomeric (stereoelectronic) effect is the predominant parameter that determines the conformation of the 3-substituted 2,4-dioxa-3-phosphadecalin 3-oxides. In the 3-axially substituted 3-fluoro-2,4-dioxa-8-aza-3-phosphadecalins **10a** and **11a**, both the steric and the anomeric effects act in the same direction. According to the vicinal couplings ($^3J(P,H_{eq}–C(5)) = 24.8$ Hz (**10a**) and $^3J(P,H_{eq}–C(5)) = 24.5$ Hz (**11a**), resp.)[3]), these compounds adopt a double-chair conformation (**C-1**)[4])[5]) (*Scheme 4*).

In the equatorial epimers **10b** and **11b**, the steric and the stereoelectronic effects are opposite. Although the chair conformation is sterically favored, the anomeric preference drives the strongly electronegative F-substituent into the stereoelectronically favored axial position, hence resulting in non-chair conformations such as boat or twist-boats (*i.e.*, **B**, **TB-1**, and **TB-2**)[4]) of the 2,4-dioxa-3-phospha moiety (*Scheme 4*)[6]). According to the vicinal-coupling data ($^3J(P,H–C(1)) = 2$, $^3J(P,H_{ax}–C(5)) = 11.5$, $^3J(P,H_{eq}–C(5)) = 10.2$ Hz), and on the basis of our recent conformational studies on the type-**III** [11–13] and type-**IV** congeners [10][12][13] (*Scheme 1*) that lead to the conformational assignments of the type-**I** inhibitors [1], we conclude in analogy that the *trans*-configured epimers (+)- and (−)-**10b** exist in an equilibrium mixture of **C-1** and **TB-2** (*Scheme 4*)[7]).

In the *cis*-configured equatorial epimers (+)- and (−)-**11b**, the flexibility of the decalin system combined with the anomeric preference of the *P(3)*-equatorial F-substituent render the situation significantly more complex, and additional conformations must be envisaged. In particular, the bicyclic system can undergo complete ring

---

[3]) Generally, the ^{31}P-NMR resonance of the axial epimer is shifted upfield with respect to the equatorial one and the chemical shift difference ($\Delta\delta = \delta_{eq} - \delta_{ax}$) is > 0, and its magnitude is inversely proportional to the electronegativity of the substituent at the P-atom. However, the cyclic phosphorofluoridates of the *cis*-series of the type **I**–**IV** compounds (*Scheme 1*, X = F) display $\Delta\delta < 0$, a fact that is only explained by significant conformational changes. The magnitude of the $^3J(P,H)$ in the ^{1}H-coupled ^{31}P-NMR is indicative of the conformation of the 2,4-dioxa-3-phospha moiety: Diagnostically relevant values for the axial epimers are $^3J(P,H_{eq}–C(5))$ *ca.* 25 Hz and $^3J(P,H_{ax}–C(5))$ *ca.* 0, whereas the equatorial ones display $^3J(P,H_{ax}–C(5)) \approx {}^3J(P,H_{eq}–C(5)) \approx 10–15$ Hz. Hence, the axial epimers exhibit a *d*-type and the equatorial ones a *m*-type splitting pattern (see [11]).

[4]) The short terms for the conformations (IUPAC convention) were introduced in [11]: **C** = chair, **B** = boat, **E** = envelope, **TB** = twist-boat (see also [1])

[5]) There is no evidence for the completely inverted **C-2** conformation in **11a**. Hence, we assume that the strong anomeric preference prevents this interconversion

[6]) In such systems, the resulting minimum-energy conformations represent a balance between the anomeric effect favoring the axial orientation in the twist-boat and the 1,3-steric and eclipsing interactions favoring the chair conformation. This fact explains the unusual stabilization of non-chair conformations.

[7]) Since $^3J(P,H–C(1))$ is *ca.* 0, conformations **B** and **TB-1** are excluded. At room temperature, the ^{31}P-NMR spectra are well resolved and coalescence phenomena are not observed, *i.e.*, the interconversion **C-1** $\rightleftharpoons$ **TB-2** is fast on the NMR time scale. In contrast to [11–13], the conformational assignments are tentative and not corroborated by variable-temperature NMR experiments nor by X-ray crystallographic analyses.

Scheme 4

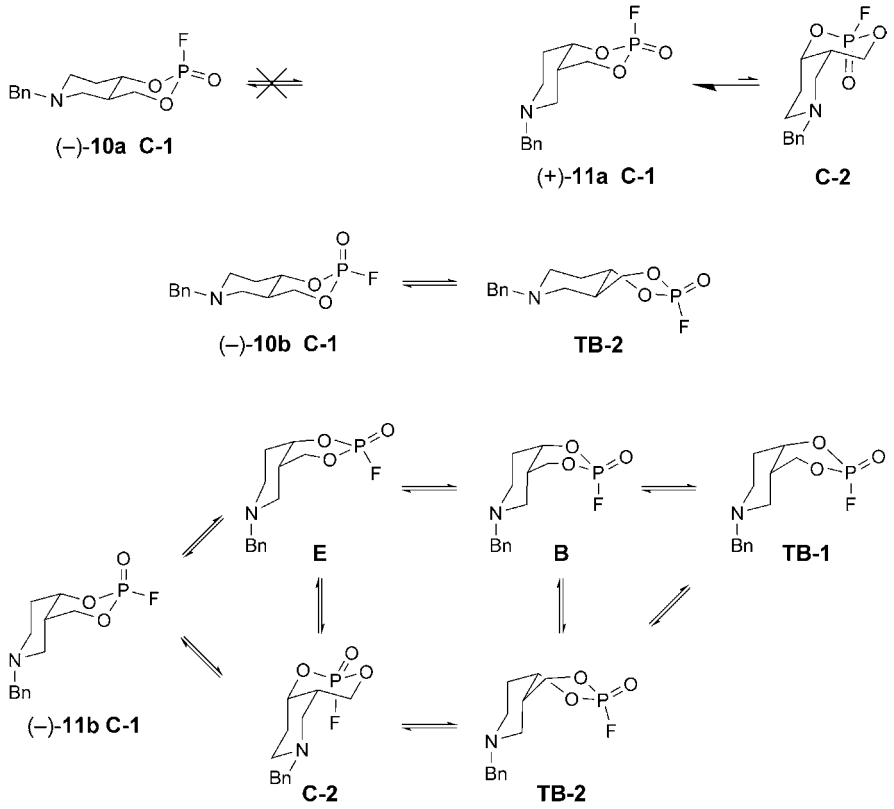

inversion to yield the prominent **C-2** arrangement (*Scheme 4*), which seems to be favored by both the anomeric and the steric effects. Moreover, although the piperidine moiety lacks stereoelectronic impact, the conformational equilibrium is also influenced by the *N*-benzyl group. According to crystal structures (see [1][11], and *Fig. 2* below), the piperidine moiety adopts a chair conformation in solution with the *N*-benzyl group in an equatorial position. However, its steric demand certainly affects the equilibrium population of the conformers, and it may interfere with a complete ring inversion to **C-2**. With regard to the experimental $^3J(P,H_{eq}–C(5)) = {}^3J(P,H–C(1)) = 18.5$ and $^3J(P,H_{ax}–C(5)) = 7.5$ Hz, none of the conformations depicted in *Scheme 4* can be excluded, nor can any be assigned[8]). Hence, we assume that **11b** exists in solution as a complex mixture of **C-1**/**C-2**, and/or **TB-1**/**TB-2**, and most likely, also **B** and envelope **E** have to be considered[9]). A full account of our detailed conformational studies on the 3-fluoro-2,4-dioxa-3-phosphadecalin 3-oxides (types **I**–**IV**) will be presented later [12].

---

[8]) The most striking argument for the exclusion of a prominent conformation is that none of the $^3J(P,H)$ is *ca.* 0, see [11].

[9]) As discussed for **10b**, the conformational assignments are tentative, and the interconversions must be fast on the NMR time scale at room temperature.

2.4. *Crystallographic Analyses of* (−)-**10a** and (−)-**11a**[10]. The structures of (−)-**10a** and (−)-**11a** were solved and refined successfully. Both compounds in the crystal were enantiomerically pure, and the absolute configurations of the molecules were determined independently by the diffraction experiments. The refinement of the absolute structure parameter confidently confirmed that the refined coordinates (*cf. Table 2*, *Exper. Part*) represent the true enantiomorphs with the expected (1*S*,3*S*,6*R*)-configuration for (−)-**10a** (*Fig. 1*), and the (1*R*,3*R*,6*R*)-configuration for (−)-**11a** (*Fig. 2*). These results independently corroborate the configurational assignments of the precursors (+)-(3*R*,4*S*)-1-benzyl-3-(hydroxymethyl)piperidin-4-ol ((+)-**2**) and (−)-(3*R*,4*R*)-1-benzyl-3-(hydroxymethyl)piperidin-4-ol ((−)-**3**) by means of the high-field ^{1}H-NMR *Mosher* method. As discussed above, the six-membered ring containing the P-atom has an undistorted chair conformation with the F-atom in the axial position, and the *N*-benzyl group occuppies the sterically favored equatorial position.

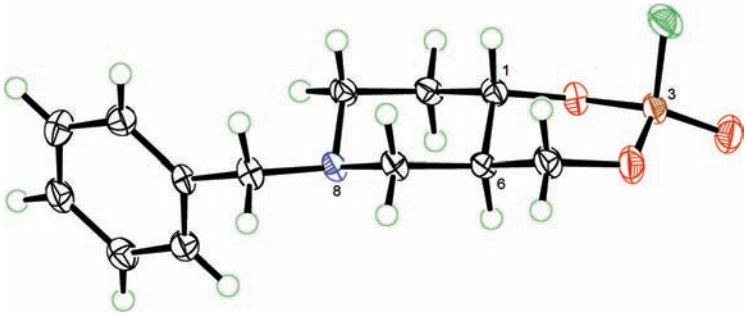

Fig. 1. *Molecular structure of* (−)-**10a** ((1*S*,3*S*,6*R*)). Trivial numbering; 50% probability ellipsoids.

All attempts to crystallize one of the equatorial epimers (+)- or (−)-**10b** and/or (+)- or (−)-**11b** resulted in complete epimerization. Hence, no X-ray crystallographic analysis of the equatorial compounds is available.

3. Enzyme Kinetics. – 3.1. *General*. The inhibitory potency and the mode of action of the enantiomerically pure 3-fluoro-2,4-dioxa-8-aza-3-phosphadecalins **10** and **11** was determined according to the general considerations and procedure explicitely described in the precedent article [1]. In particular, the data acquisition was based on the *Ellman* assay [14]) and the mathematical evaluation was performed according to [15]. For irreversible inhibition, the simplified overall processes were considered that directly yield the covalently phosphorylated enzyme ***E–I*** (*Scheme 5*, mechanism *a*) or involve a preceding reversible step *via* the associative complex ***E*·*I**** (*Scheme 5*, mechanism *b*) [1]. However, since several congeners of the 3-fluoro-2,4-dioxo-8-aza-3-phosphadecalins were reversible inhibitors of AChE, the basic equilibria that govern the formation of the adsorptive complexes ***EI***, ***ES***, and ***ESI*** had to be considered, too (*Scheme 5*, mechanism *c*) [16].

[10]) The full data sets are summarized in *Table 2* (see *Exper. Part*). CCDC-838432 ((−)-**10a**) and CCDC-838433 ((−)-**11a**) contain supplementary crystallographic data. These can be obtained free of charge from the *Cambridge Crystallographic Data Centre via* www.code.cam.ac.uk/data_request/cif.

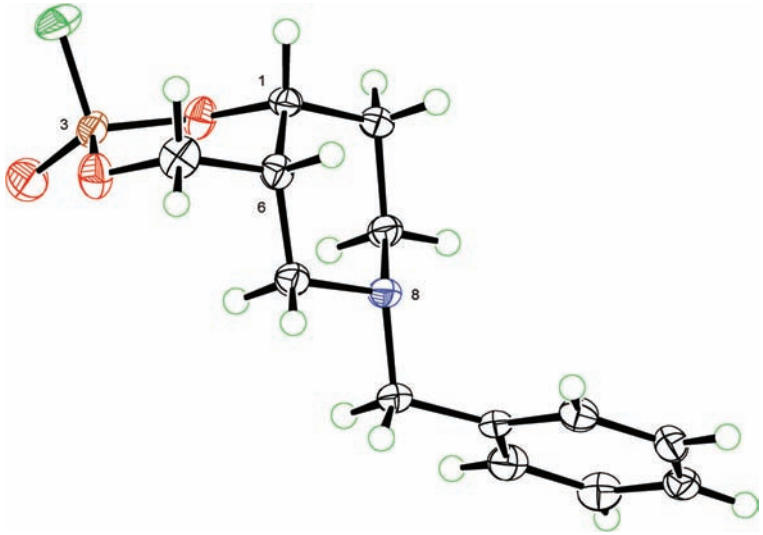

Fig. 2. *Molecular structure of* (−)-**11a** ((1*R*,3*R*,6*R*)). Trivial numbering; 50% probability ellipsoids.

3.2. *Data Analysis and Results.* Determination of the apparent rate constants (k_{obs}) from the progress curves ($A = f(t)$, see *Eqn. 1* in the *Exper. Part*) and the mathematical evaluation of the dependence $k_{obs} = f([\boldsymbol{I}])$ to evaluate the irreversible inhibition parameters (K_D, k_a, k_i, and k_p) are performed according to [15]. The reversible inhibition parameters (K_I and K'_I) were determined from the linear primary plots ($A = f(t)$) by application of approved linearization procedures [16][17]. The mathematical equations (*Eqns. 1–3*) underlying *Scheme 5* and further details are summarized in the *Exper. Part*. The secondary plot ($k_{obs} = f([\boldsymbol{I}])$) exhibited a linear dependence for (±)-**10a**, (+)-**10a**, and mechanism *a* was assigned. In the case of (+)- and (−)-**10b**, (−)-**11a**, and (+)- and (−)-**11b**, the secondary plot depended hyperbolically upon [***I***], and mechanism *b* was assigned for these compounds. Since the primary plots ($A = f(t)$) for (−)-**10a** and (+)-**11a** clearly displayed a linear dependence, these compounds are reversible inhibitors of AChE. According to the comparison of the results of the different linearization methods [2], the linear mixed inhibition mechanism *c* could be assigned (*Scheme 5*)[11]). The experimental results are summarized in *Table 1*.

Compared to the potent standard reference diisopropyl phosphorofluoridate ($P(O)F(O^iPr)_2$) and both the type-**I** [1] and type-**IV** [10] congeners, the investigated 3-fluoro-2,4-dioxa-8-aza-3-phosphadecalins **10** and **11** are very weak inhibitors of AChE, the most potent compound (+)-**10a** being only half as active as the weakest type-**I** inhibitor. The *P(3)*-equatorially subsituted congeners (+)- and (−)-**10b** and (+)- and (−)-**11b** react according to mechanism *b* and do not display significant stereoselectivity. In contrast, the *P(3)*-axially substituted pairs (+)- and (−)-**10a** and (+)- and (−)-**11a** are remarkably enantioselective. Whereas (+)-**10a** phosphorylates AChE directly (mechanism *a*), its enantiomer (−)-**10a** is a reversible inhibitor (mechanism *c*).

---

[11]) However, the results of the linearization processes were not fully distinct [2], see *Exper. Part*.

Scheme 5

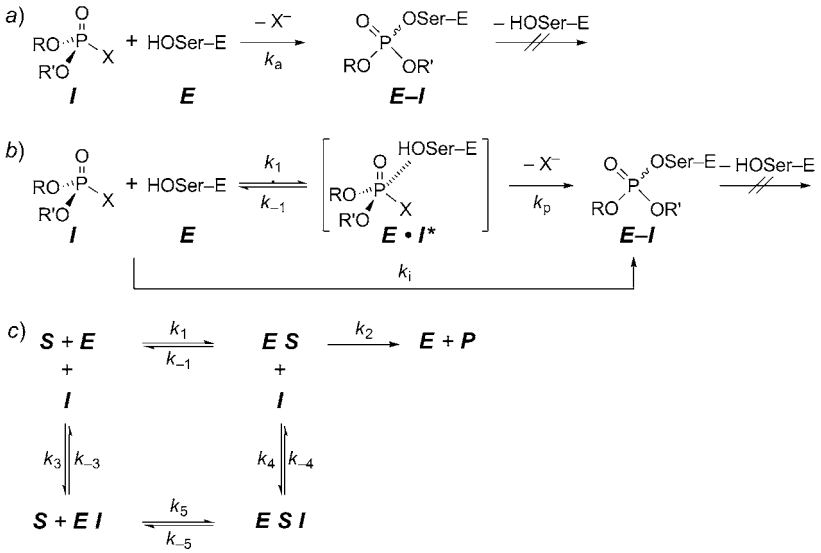

E = Free enzyme: serine hydrolase (acetylcholinesterase, chymotrypsin)
I = Inhibitor, ***S*** = substrate, ***P*** = product(s)
k_a: Association constant
$k_{-1}/k_1 = K_D$: Dissociation constant (also referred to as K_S)
k_p: Phosphorylation constant
$k_i = k_p/K_D$: Overall inhibitory potency ('bimolecular reaction constant')
k_2: First-order rate constant
$k_{-3}/k_3 = K_I$: Competitive inhibition constant (also referred to as K_{ic})
$k_{-4}/k_4 = K'_I$: Noncompetitive inhibition constant ($K'_I = \alpha K_I$, also referred to as K_{iu})
$k_{-5}/k_5 = K'_S$: Triple complex association constant ($K'_S = \alpha K_S$, also referred to as K_{Ai})
$\alpha = (1 + [I])/K_I = [S]/[S] + K_m$: modifying factor
$K_I = K'_I$, $K_S = K'_S$: Noncompetitive Inhibition
$K_I \neq K'_I$, $K_S \neq K'_S$: Linear mixed-type inhibition

Table 1. *Kinetic Data of the Inhibition of AChE with the Enantiomerically Pure 3-Fluoro-2,4-dioxa-8-aza-3-phosphadecalins (+)- and (−)-***10** *and (+)- and (−)-***11** ($P(O)F(O^iPr)_2$ as reference)

	Kinetic parameters	Mechanism		Kinetic parameters	Mechanism
(+)-**10a**	$k_a = 4.3 \pm 0.1\ M^{-1}s^{-1}$	*a*	(+)-**11a**	$K_i = 930 \pm 5\ \mu M$	*c*
(−)-**10a**	$K_i = 1'600 \pm 20\ \mu M$	*c*		$K'_i = 7'600 \pm 30\ \mu M$	
	$K'_i = 1'750 \pm 20\ \mu M$		(−)-**11a**	$k_i = 18.5 \pm 0.7\ M^{-1}s^{-1}$	*b*
(±)-**10a**	$k_a = 1 \pm 0.1\ M^{-1}s^{-1}$	*a*		$K_D = 40 \pm 5\ \mu M$	
(+)-**10b**	$k_i = 31.7 \pm 0.3\ M^{-1}s^{-1}$	*b*		$k_p = 0.0007 \pm 0.00003\ s^{-1}$	
	$K_D = 105 \pm 6\ \mu M$		(+)-**11b**	$k_i = 75.0 \pm 0.5\ M^{-1}s^{-1}$	*b*
	$k_p = 0.0033 \pm 0.0004\ s^{-1}$			$K_D = 100 \pm 5\ \mu M$	
(−)-**10b**	$k_i = 23.3 \pm 0.4\ M^{-1}s^{-1}$	*b*		$k_p = 0.0075 \pm 0.0001\ s^{-1}$	
	$K_D = 73 \pm 5\ \mu M$		(−)-**11b**	$k_i = 48.3 \pm 0.5\ M^{-1}s^{-1}$	*b*
	$k_p = 0.0017 \pm 0.0001\ s^{-1}$			$K_D = 52 \pm 5\ \mu M$	
				$k_p = 0.0025 \pm 0.0003\ s^{-1}$	
			$P(O)F(O^iPr)_2$	$k_a = 195 \pm 3\ M^{-1}s^{-1}$	*a*

Interestingly, its racemate (±)-**10a** reacts irreversibly (mechanism *a*), thus confirming the finding that the inhibitory activity of a racemic inhibitor is roughly the arithmetic mean of the enantiomers [13][12]). Similarly, (−)-**11a** is an irreversible inhibitor of AChE (mechanism *b*), whereas (+)-**11a** reacts reversibly with the enzyme (mechanism *c*). However, since all compounds are very weak inhibitors of AChE, a clear differentiation of the primary plot type ($A = f(t)$) was not always straightforward[11]). In particular, in some cases its curvature was not too pronounced and rather converged towards a straight line as is characteristic for reversible inhibitors. Therefore, the interpretation and assignment of mechanism *c*) is not fully assured[13]).

4. Remarks. – Besides the investigation of the stereochemical implications of the inhibition reaction by ^{31}P-NMR spectroscopy [5–7][13], it is the aim of our research project to study the molecular interactions of AChE with acetylcholine (ACh). In particular, kinetic studies are performed to deliver insight into the physiologically active (recognition) conformation of ACh that governs the enzymatic hydrolysis process[14]). Being γ-homoacetylcholine mimetics, the 8-benzyl-3-fluoro-2,4-dioxa-8-aza-3-phosphadecalin 3-oxides **10** and **11** (type-**II** inhibitors) clearly differ from the natural substrate. They cannot be compared directly with ACh and are not able to adopt a respective recognition conformation. Hence, the disclosed very weak inhibitory potency is not surprising. Moreover, the *N*-benzyl group as additional structural feature is considered to influence both the steric demand and the basicity of the compound. In particular, the cationic site of ACh is substituted by an electron donating group. However, in spite of these restrictions, the actual results provide some evidence of the viability of our concept[15]), but they do not allow to draw significant further conclusions.

The authors are indebted to PD Dr. *A. Linden*, head of the X-ray department of our institute, for the high-quality X-ray crystallographic analyses. The financial support of the project by the *Swiss National Science Foundation* is gratefully acknowledged.

Experimental Part

1. *General*. See [1][3][6]. For the particular precautions in preparing and handling the organophosphates, see [3]. Determination of ee: based on the integration of the peak areas of the anal. HPLC separations of the precursor diols with optimized resolution ($R_s > 4$). NMR Assignments: based on extensive 2D-NMR (see [3]) and selective ^{1}H-decoupling experiments.

---

12) Although apparently obvious, it cannot be concluded *a priori* that the inhibition constants are simply additive.

13) Meanwhile, we have presented a novel, integrated approach with a reappraisal of kinetic mechanisms and diagnostic methods that enables distinct as well as subtle differentiations of generalized inhibition mechanisms [18]. Because the kinetic experiments and the data evaluation for the (+)- and (−)-9-benzyl-3-fluoro-2,4-dioxa-8-aza-3-phosphadecalin 3-oxides **10** and **11** were performed earlier [2] than the recent findings [18], the analysis of the assay data follows the simplified procedure according to [15]. A complete re-interpretation of the kinetic data of **10** and **11** is in process [19].

14) Concerning a discussion on the recognition conformation of ACh, see [1].

15) At least, our working hypothesis is not discredited by this negative evidence.

2. *(+)-(3*R,*4*S*)- and (−)-(3*S,*4*R*)-, and (+)-(3*S,*4*S*)- and (−)-(3*R,*4*R*)-1-Benzyl-3-(hydroxymethyl)-piperidin-4-ols* (=*corresponding 4-Hydroxy-1-(phenylmethyl)piperidine-3-methanols*; (+)- and (−)-**2**, and (+)- and (−)-**3**, resp.). The precursor diols were prepared and characterized as described earlier [3][8]. The absolute configurations were assigned by means of the high field ^{1}H-NMR *Mosher* method [9] applied to the (*R*)- and (*S*)-MTPA ester couples **6a**/**6b**, **7a**/**7b**, **8a**/**8b**, and **9a**/**9b**; for explicit details, see [2][8].

3. trans- *and* cis-*8-Benzyl-3-fluoro-2,4-dioxa-8-aza-3-phosphadecalin 3-Oxides* (=*2-Fluorohexahydro-6-(phenylmethyl)-4*H-*1,3,2-dioxaphosphorino[5,4-*c*]pyridine 2-Oxides*) *(+)- and (−)-***10a***, (+)- and (−)-***10b***, (+)- and (−)-***11a***, and (+)- and (−)-***11b***, resp.* To a cooled soln. (−5°) of (−)-**2** (136 mg, 0.61 mmol) in anh. CH_2Cl_2 (2.5 ml) in a glove box (N_2 atmosphere), a cooled soln. (−5°) of $POCl_2F$ [20] (62 µl, 0.68 mmol, 1.11 equiv.) in Et_2O (2 ml) was added with a syringe, and the mixture was stirred for 5 min at 0° when the mixture was withdrawn and quickly passed through SiO_2 (SiO_2 *60*, 15–40 µm (*Merck*, *115111*), pH 5.6 [6], Et_2O). The eluate was gently evaporated (N_2 stream, <30°), and the residue ((+)-**10a**/(+)-**10b**, ax/eq *ca.* 1:1; 167 mg) was subjected to CC (SiO_2, pH 5.6 [6], Et_2O): (+)-**10a** (48 mg, 28%) and (+)-**10b** (43 mg, 25%). Applying the same procedure, phosphorylation of (+)-**2** (98 mg, 0.44 mmol) afforded (−)-**10a** (34 mg, 27%) and (−)-**10b** (22 mg, 17%); the axial epimers were less polar.

Similarly, the *cis*-configured compounds were obtained after phosphorylation and CC (SiO_2, pH 5.6 [6], hexane/AcOEt 1:2 containing 3.5% MeOH): from (+)-**3** (132 mg, 0.59 mmol), (+)-**11a** (62 mg, 37%) and (−)-**11b** (39.2 mg, 41%); from (−)-**3** (162 mg, 0.61 mmol), (−)-**11a** (81 mg, 43%) and (+)-**11b** (64 mg, 37%); the equatorial epimers were less polar.

In contrast to the racemic compounds [3], the optically active *P(3)*-equatorially substituted 3-fluoro-2,4-dioxa-8-aza-3-phosphadecalins partially epimerized during CC. Therefore, the contact time to SiO_2 had to be minimized by an optimized adsorbent/substance ratio (*ca.* 25 mg on a 8 × 1 cm column) and high flow rates (*ca.* 4 ml/min). However, although the operating conditions were optimized, (+)- and (−)-**10b** contained *ca.* 4–5% of (+)- and (−)-**10a** [2]. The axial epimers were stable when stored as such (<0°, Ar), but in soln. they slowly decomposed. Although being resonably stable when stored as such (<0°, Ar), the equatorial epimers gradually epimerized; in particular, the *trans*-congeners (+)- and (−)-**10b** completely epimerized during crystallization to yield (+)- and (−)-**10a**, resp. [2].

*(+)-(1*R,*3*R,*6*S*)-8-Benzyl-3-fluoro-2,4-dioxa-8-aza-3-phosphadecalin 3-Oxide* (=*(+)-(2*R,*4a*S,*8a*R*)-2-Fluorohexahydro-6-(phenylmethyl)-4*H-*1,3,2-dioxaphosphorino[5,4-*c*]pyridine 2-Oxide*; (+)-**10a**): Colorless prisms. M.p. 174–175.5°. R_f (Et_2O) 0.37. $[\alpha]_D = +30.3$ ($c = 1.00$, acetone; ee > 99%). IR (KBr): 3008*w*, 3060*w*, 3026*m*, 2961*m*, 2938*m* 2869*w*, 2820*m*, 2805*m*, 2778*m*, 2728*w*, 1493*m*, 1486*w*, 1471*w*, 1449*m*, 1393*w*, 1368*w*, 1322*s*, 1264*w*, 1218*m*, 1182*m*, 1142*m*, 1134*w*, 1105*m*, 1074*w*, 1045*s*, 997*s*, 968*m*, 915*m*, 899*s*, 846*w*, 799*m*, 786*m*, 741*m*, 698*m*, 663*m*, 535*m*. ^{1}H-NMR (400 MHz, $CDCl_3$): 7.36–7.25 (*m*, *Ph*CH_2); 4.29 (*A* of *ABX-P*, $^2J = 11.0$, ^3J(5eq,P) = 24.5, ^3J(5eq,6) = 4.5, H_{eq}–C(5)); 4.18 (*td*, $^3J(1,6) = {}^3J(1,10ax) = 12.0$, $^3J(1,10eq) = 4.8$, H–C(1)); 4.11 (*B* of *ABX-P*, $^2J = {}^3J(5ax,6) = 11.0$, $^3J(5ax,P) = 1.0$, H_{ax}–C(5)); 3.58, 3.47 (*AB*, $^2J = 13.2$, PhCH_2); 3.01 (*dddd*, $^2J = 12.0$, $^3J(9eq,10ax) = 4.5$, $^3J(9eq,10eq) = 2.5$, $^4J(9eq,7eq) = 2.2$, H_{eq}–C(9)); 2.81 (*ddd*, $^2J = 11.2$, $^3J(7eq,6) = 3.8$, $^4J(7eq,9eq) = 2.2$, H_{eq}–C(7)); 2.34 (*X* of *ABX-P*, $^3J(6,1) = 12.0$, $^3J(6,5ax) = 11.0$, $^3J(6,5eq) = 4.5$, $^3J(6,7ax) = 11.2$, $^3J(6,7eq) = 3.8$, H–C(6)); 2.12 (*td*, $^2J = {}^3J(9ax,10ax) = 12.0$, $^3J(9ax,10eq) = 2.5$, H_{ax}–C(9)); 2.08 (*ddt*, $^2J = 12.0$, $^3J(10eq,1) = 4.8$, $^3J(10eq,9ax) = {}^3J(10eq,9eq) = 2.5$, H_{eq}–C(10)); 1.94 (*qd*, $^2J = {}^3J(10ax,1) = {}^3J(10ax,9ax) = 12.0$, $^3J(10ax,9eq) = 4.5$, H_{ax}–C(10)); 1.70 (*t*, $^2J = {}^3J(7ax,6) = 11.2$, H_{ax}–C(7)). ^{13}C-NMR (100.6 MHz, $CDCl_3$): 137.4 (C(1′)); 128.7 (C(2′), C(6′)); 128.3 (C(3′), C(5′)); 127.4 (C(4′)); 83.0 (*d*, $^2J(1,P) = 6.5$, C(1)); 71.8 (*d*, $^2J(5,P) = 7.6$, C(5)); 62.9 (Ph*C*H_2); 51.1 (C(9)); 51.0 (C(7)); 39.6 (*d*, $^3J(6,P) = 6.2$, C(6)); 31.6 (*d*, $^3J(10,P) = 9.2$, C(10)). ^{31}P-NMR (161.9 MHz, $CDCl_3$): −15.9 (*dd*, $^1J(P,F) = 1010$, $^3J(P,H_{eq}$–C(5)) = 24.5. ^{19}F{^{1}H}-NMR (376.5 MHz, $CDCl_3$): −85.3 (*d*, $^1J(F,P) = 1010$). EI-MS: 285 (25, M^+), 208 (8), 194 (10, $[M - PhCH_2]^+$), 186 (14), 185 (13), 172 (12), 146 (3), 132 (8), 126 (17), 118 (4), 94 (23), 92 (25), 91 (100, $PhCH_2^+$), 67 (5), 65 (17), 56 (3).

*(−)-(1*S,*3*S,*6*R*)-8-Benzyl-3-fluoro-2,4-dioxa-8-aza-3-phosphadecalin 3-Oxide* (=*(−)-(2*S,*4a*R,*8a*S*)-2-Fluorohexahydro-6-(phenylmethyl)-4*H-*1,3,2-dioxaphosphorino[5,4-*c*]pyridine 2-Oxide*; (−)-**10a**): $[\alpha]_D = -28.9$ ($c = 1.00$, acetone; ee > 98%)[2]. All other data: identical with those of (+)-**10a**.

*(+)-(1*R,*3*S,*6*S*)-8-Benzyl-3-fluoro-2,4-dioxa-8-aza-3-phosphadecalin 3-Oxide* (=*(+)-(2*S,*4a*S,*8a*R*)-2-Fluorohexahydro-6-(phenylmethyl)-4*H-*1,3,2-dioxaphosphorino[5,4-*c*]pyridine 2-Oxide*; (+)-**10b**):

Colorless prisms. M.p. 113–114°[16]). R_f (Et_2O): 0.29. $[\alpha]_D^{25} = +47.5$ ($c = 1.00$, acetone; ee > 99%). IR (KBr): 3065*w*, 3028*w*, 2978*w*, 2920*w*, 2869*w*, 2823*m*, 2780*w*, 1605*w*, 1498*m*, 1479*w*, 1455*m*, 1393*m*, 1368*m*, 1345*s*, 1327*s*, 1280*w*, 1205*w*, 1183*w*, 1178*w*, 1148*w*, 1131*w*, 1109*m*, 1085*m*, 1069*m*, 1042*s*, 999*m*, 975*m*, 959*m*, 915*m*, 897*s*, 849*m*, 772*m*, 705*w*, 635*m*, 575*m*. ^{1}H-NMR (400 MHz, $CDCl_3$): 7.36–7.25 (*m*, *Ph*CH_2); 4.37 (*A* of *ABX-P*, $^2J = 11.5$, $^3J(5eq,P) = 10.2$, $^3J(5eq,6) = 5.7$, H_{eq}–C(5))[17]); 4.31 (*tdd*, $^3J(1,10ax) = {}^3J(1,6) = 11.5$, $^3J(1,10eq) = 4.5$, $^4J(1,F) = 2.0$, H–C(1)); 4.13 (*B* of *ABX-P*, $^2J = {}^3J(5ax,P) = 11.5$, $^3J(5ax,6) = 10.5$, $^4J(5ax,F) = 3.7$, H_{ax}–C(5))[17]); 3.58, 3.46 (*AB*, $^2J = 13.2$, PhCH_2); 3.01 (*dddd*, $^2J = 11.5$, $^3J(9eq,10ax) = 4.5$, $^3J(9eq,10eq) = 2.5$, $^4J(9eq,7eq) = 2.2$, H_{eq}–C(9)); 2.84 (*ddd*, $^2J = 11.0$, $^3J(7eq,6) = 3.8$, $^4J(7eq,9eq) = 2.2$, H_{eq}–C(7)); 2.48 (*X* of *ABX-P*, $^3J(6,1) = 11.5$, $^3J(6,5ax) = 10.5$, $^3J(6,5eq) = 5.7$, $^3J(6,7ax) = 11.0$, $^3J(6,7eq) = 3.8$, H–C(6)); 2.15 (*dtd*, $^2J = 11.5$, $^3J(10eq,1) = {}^3J(10eq,9eq) = 4.5$, $^3J(10eq,9ax) = 2.5$, H_{eq}–C(10)); 2.12 (*td*, $^2J = {}^3J(9ax,10ax) = 11.5$, $^3J(9ax,10eq) = 2.5$, H_{ax}–C(9)); 1.90 (*qd*, $^2J = {}^3J(10ax,1) = {}^3J(10ax,9ax) = 11.5$, $^3J(10ax,9eq) = 4.2$, H_{ax}–C(10)); 1.72 (*t*, $^2J = {}^3J(7ax,6) = 11.0$, H_{ax}–C(7)). ^{13}C-NMR (100.6 MHz, $CDCl_3$): 137.4 (C(1′)); 128.7 (C(2′), C(6′)); 128.3 (C(3′), C(5′)); 127.4 (C(4′)); 82.3 (*d*, $^2J(1,P) = 6.6$, C(1)); 71.4 (*d*, $^2J(5,P) = 7.1$, C(5)); 62.0 (PhCH_2); 52.0 (C(7)); 51.0 (C(9)); 38.5 (*d*, $^3J(6,P) = 12.6$, C(6)); 32.0, $^3J(10,P) = 7.1$ (C(10)). ^{31}P-NMR (161.9 MHz, $CDCl_3$): −15.4 (*dddt*, $^1J(P,F) = 998$, $^3J(P,H_{ax}$–C(5)) = 11.5, $^3J(P,H_{eq}$–C(5)) = 10.2, $^3J(P,H$–C(1)) = $^4J(P,H$–C(6)) = 2)[17]). ^{19}F{^{1}H}-NMR (376.5 MHz, $CDCl_3$): −69.3 (*d*, $^1J(F,P) = 998$). EI-MS: 285 (22, M^+), 208 (10), 194 (32, $[M - PhCH_2]^+$), 186 (6), 172 (3), 160 (3), 132 (8), 126 (16); 112 (18), 94 (15), 92 (25), 91 (100, $PhCH_2^+$), 67 (10), 65 (15), 55 (5).

*(−)-(1*S*,3*R*,6*R*)-8-Benzyl-3-fluoro-2,4-dioxa-8-aza-3-phosphadecalin 3-Oxide* (= *(−)-(2*R*,4a*R*,8a*S*)-2-Fluorohexahydro-6-(phenylmethyl)-4*H*-1,3,2-dioxaphosphorino[5,4-*c*]pyridine 2-Oxide*; (−)-**10b**): $[\alpha]_D = -42.3$ ($c = 1.00$, acetone; ee > 98%)[2]). All other data: identical with those of (+)-**10b**.

*(+)-(1*S*,3*S*,6*S*)-8-Benzyl-3-fluoro-2,4-dioxa-8-aza-3-phosphadecalin 3-Oxide* (= *(+)-(2*S*,4a*S*,8a*S*)-2-Fluorohexahydro-6-(phenylmethyl)-4*H*-1,3,2-dioxaphosphorino[5,4-*c*]pyridine 2-Oxide*; (+)-**11a**): Colorless prisms. M.p. 111.5–113°. R_f (AcOEt/MeOH 98:2) 0.20. $[\alpha]_D = +47.0$ ($c = 1.00$, acetone; ee > 99%). IR (KBr): 3088*w*, 3065*w*, 3029*w*, 2968*m*, 2920*m*, 2908*m*, 2833*w*, 2808*m*, 2779*m*, 1500*w*, 1479*w*, 1456*w*, 1424*w*, 1386*w*, 1372*w*, 1366*w*, 1355*w*, 1338*m*, 1311*s*, 1278*w*, 1212*m*, 1161*w*, 1125*w*, 1099*m*, 1077*s*, 1048*m*, 1028*s*, 987*s*, 973*m*, 952*m*, 915*m*, 893*s*, 835*m*, 790*w*, 773*m*, 739*m*, 726*m*, 642*m*, 509*m*. ^{1}H-NMR (400 MHz, $CDCl_3$): 7.35–7.23 (*m*, *Ph*CH_2); 4.87 (*qd*-like, $^3J(1,6) = {}^3J(1,10ax) = {}^3J(1,10eq) = 2.6$, $^4J(1,P) = 1.5$, H–C(1)); 4.53 (*A* of *ABX-P*, $^2J = 11.7$, $^3J(5ax,P) < 1$, $^3J(5ax,6) = 2.9$, H_{ax}–C(5)); 4.22 (*B* of *ABX-P*, $^2J = 11.7$, $^3J(5eq,P) = 24.8$, $^3J(5eq,6) < 1$, H_{eq}–C(5)); 3.60, 3.50 (*AB*, $^2J = 13.0$, PhCH_2); 2.72 (*dquint.*-like, $^2J = 11.8$, $^3J(9eq,10ax) \approx {}^3J(9eq,10eq) = 2.4$, $^4J(9eq,7eq) = 1.0$, H_{eq}–C(9)); 2.69 (*ddd*, $^2J = 11.8$, $^3J(7eq,6) = 4.6$, $^4J(7eq,9eq) = 1.0$, H_{eq}–C(7)); 2.54 (*t*, $^2J = {}^3J(7ax,6) = 11.8$, H_{ax}–C(7)); 2.39 (*td*, $^2J = {}^3J(9ax,10ax) = 11.8$, $^3J(9ax,10eq) = 3.2$, H_{ax}–C(9)); 2.06 (*X* of *ABX-P*, $^3J(6,1) = 2.6$, $^3J(6,5ax) = 2.9$, $^3J(6,5eq) < 1$, $^3J(6,7ax) = 11.8$, $^3J(6,7eq) = 4.6$, $^4J(6,P) = 1.5$, H–C(6)); 2.01 (br. *dddd*, $^2J = 14.5$, $^3J(10eq,1) = 2.6$, $^3J(10eq,9ax) = 3.2$, $^3J(10eq,9eq) = 2.4$, $^4J(10eq,P) \approx 1$, H_{eq}–C(10)); 1.96 (*qdd*-like, $^2J = 14.5$, $^3J(10ax,1) = 2.6$, $^3J(10ax,9ax) = 11.8$, $^3J(10ax,9eq) = 2.4$, $^4J(10ax,P) = 6.0$, H_{ax}–C(10)). ^{13}C-NMR (100.6 MHz, $CDCl_3$): 137.9 (C(1′)); 129.0 (C(2′), C(6′)); 128.3 (C(3′), C(5′)); 127.3 (C(4′)); 78.5 (*dd*, $^2J(1,P) = 7.3$, $^3J(1,F) = 1.5$, C(1)); 72.3 (*d*, $^2J(5,P) = 6.9$, C(5)); 62.9 (PhCH_2); 49.5 (C(7)); 46.7 (C(9)); 35.5 (*d*, $^3J(6,P) = 5.9$, C(6)); 31.0 (*d*, $^3J(10,P) = 8.8$, C(10)). ^{31}P-NMR (161.9 MHz, $CDCl_3$): −16.6 (*ddd*, $^1J(P,F) = 1009$, $^3J(P,H_{eq}$–C(5)) = 24.8, $^4J(P,H_{ax}$–C(10)) = 6.0, $^4J(P,H$–C(1)) = $^4J(P,H$–C(6) = 1.5). ^{19}F{^{1}H}-NMR (376.5 MHz, $CDCl_3$): −85.1 (*d*, $^1J(F,P) = 1009$). EI-MS: 285 (22, M^+), 208 (11), 194 (28, $[M - PhCH_2]^+$), 172 (6), 144 (5), 133 (10), 118 (7), 94 (20), 92 (23), 91 (100, $PhCH_2^+$), 67 (10), 65 (16).

---

16) The specified m.p. corresponds to (±)-**10b** [3]. As discussed above, (+)- and (−)-**10b** epimerize during the crystallization process to yield (+)- and (−)-**10a**, resp. (colorless needles, m.p. *ca.* 170–175°).

17) The descriptors 'ax' and 'eq' for the H-atoms at C(5) are based on their relative positions in the chair conformation of the 2,4-dioxa-3-phospha moiety. As discussed (*Scheme 4*), the conformation is rather a twist-boat (**TB-2**) than a chair in the *P(3)*-equatorially substituted compounds. For reasons of simplicity, the notation 'ax' and 'eq' is maintained. H_{ax}–C(5) is always *cis* to H–C(1) and H_{eq}–C(5) *trans* to H–C(1), see [11].

*(−)-(1*R*,3*R*,6*R*)-8-Benzyl-3-fluoro-2,4-dioxa-8-aza-3-phosphadecalin 3-Oxide* (=*(−)-(2*R*,4a*R*, 8a*R*)-2-Fluorohexahydro-6-(phenylmethyl)-4*H*-1,3,2-dioxaphosphorino[5,4-*c*]pyridine 2-Oxide*; (−)-**11a**): $[\alpha]_D = -46.7$ ($c = 1.00$, acetone; ee > 99%). All other data: identical with those of (+)-**11a**.

*(+)-(1*R*,3*S*,6*R*)-8-Benzyl-3-fluoro-2,4-dioxa-8-aza-3-phosphadecalin 3-Oxide* (=*(+)-(2*S*,4a*R*, 8a*R*)-2-Fluorohexahydro-6-(phenylmethyl)-4*H*-1,3,2-dioxaphosphorino[5,4-*c*]pyridine 2-Oxide*; (+)-**11b**): Colorless viscous oil. R_f (AcOEt/MeOH 98:2) 0.32. $[\alpha]_D = +18.3$ ($c = 1.00$, acetone; ee > 99%). IR (KBr): 3029*w*, 2965*m*, 2818*m*, 1495*m*, 1476*w*, 1451*m*, 1389*w*, 1330*s*, 1238*w*, 1203*w*, 1174*m*, 1133*m*, 1058*s*, 1029*s*, 1005*m*, 942*m*, 906*w*, 850*m*, 800*w*, 782w, 741*m*, 696*m*, 625*w*, 512*m*. ^{1}H-NMR (400 MHz, $CDCl_3$): 7.35–7.22 (*m*, *Ph*CH_2); 4.82 (*A* of *ABX-P*, $^2J = 11.5$, $^3J(5ax,P) = 7.5$, $^3J(5ax,6) = 4.6$, H_{ax}–C(5))[17]; 4.71 (*quint.d*-like, $^3J(1,P) = 18.5$, $^3J(1,10ax) = 9.8$, $^3J(1,6) \approx {}^3J(1,10eq) \approx {}^4J(1,F) \approx 5$, H–C(1)); 4.36 (*B* of *ABX-P*, $^2J = 11.5$, $^3J(5eq,P) = 18.5$, $^3J(5eq,6) = 4.6$, H_{eq}–C(5))[17]; 3.50, 3.40 (*AB*, $^2J = 13.0$, PhCH_2); 2.85 (*m*, br. *d*-like, $w_{1/2} \approx 22$, $^2J = 11$, H_{eq}–C(9)); 2.71 (*ddd*, $^2J = 12.5$, $^3J(7eq,6) = 3.8$, $^4J(7eq,9eq) = 1.6$, H_{eq}–C(7)); 2.51 (*X* of *ABX-P*, *quint.*-like, $w_{1/2} \approx 22$, H–C(6)); 2.32 (*dd*, $^2J = 12.5$, $^3J(7ax,6) = 3.5$, H_{ax}–C(7)); 2.25 (br. *qd*-like, $^2J \approx 12$, $^3J(10ax,9ax) \approx {}^3J(10ax,1) \approx 10$, $^3J(10ax,9eq) \approx 5$, H_{ax}–C(10)); 2.17 (br. *t*-like, $^2J \approx {}^3J(9ax,10ax) \approx 11$, H_{ax}–C(9)); 2.08 (*m*, $w_{1/2} \approx 25$, H_{eq}–C(10)). ^{13}C-NMR (100.6 MHz, $CDCl_3$): 137.8 (C(1′)); 128.6 (C(2′), C(6′)); 128.4 (C(3′), C(5′)); 127.4 (C(4′)); 80.7 (*dd*, ^2J(1,P) = 6.5, ^3J(1,F) = 2, C(1)); 70.1 (*d*, ^2J(5,P) = 6.9, C(5)); 62.1 (Ph*C*H_2); 51.7 (C(7)); 50.9 (C(9)); 35.1 (*d*, ^3J(6,P) = 8.1, C(6)); 28.5 (C(10)). ^{31}P-NMR (161.9 MHz, $CDCl_3$): −16.1 (br. *dtd*, ^1J(P,F) = 1001, ^3J(P,H–C(1)) = ^3J(P,H_{eq}–C(5))) = 18.5, ^3J(P, H_{ax}–C(5)) = 7.5)[17]). ^{19}F{^{1}H}-NMR (376.5 MHz, $CDCl_3$): −74.8 (*d*, ^1J(F,P) = 1001). EI-MS: 285 (22, M^+), 208 (11), 194 (28, $[M - PhCH_2]^+$), 172 (6), 133 (10), 132 (14), 94 (20), 92 (23), 91 (100, $PhCH_2^+$), 67 (10), 65 (16).

*(−)-(1*S*,3*R*,6*S*)-8-Benzyl-3-fluoro-2,4-dioxa-8-aza-3-phosphadecalin 3-Oxide* (=*(−)-(2*R*,4a*S*,8a*S*)-2-Fluorohexahydro-6-(phenylmethyl)-4*H*-1,3,2-dioxaphosphorino[5,4-*c*]pyridine 2-Oxide*; (−)-**11b**): $[\alpha]_D = -18.4$ ($c = 1.00$, acetone; ee > 99%). All other data: identical with those of (+)-**11b**.

4. *X-Ray Crystal-Structure Determinations of (−)-***10a** *and (−)-***11a**[10]). 4.1. *General.* All measurements were made by means of a *Nonius KappaCCD* area-detector diffractometer [21] with graphite-monochromated MoK_α radiation (λ 0.71073 Å) and an *Oxford-Cryosystems-Cryostream-700* cooler. Data reduction was performed with HKL DENZO and SCALEPACK [22]. The intensities were corrected for *Lorentz* and polarization effects, and an absorption correction based on the multi-scan method [23] was applied. Neutral-atom scattering factors for non-H-atoms were taken from [24], and the scattering factors for H-atoms were taken from [25]. Anomalous dispersion effects were included in F_c [26]; the values for f' and f'' were those of [27]. The values of the mass attenuation coefficients are those of [28]. All calculations were performed with the SHELXL97 program [29], and the crystallographic diagrams were drawn with ORTEPII [30].

4.2. *Determination of (−)-***10a**. The unit cell constants and an orientation matrix for data collection were obtained from a least-squares refinement of the setting angles of 48331 reflections in the range $4° < 2\theta < 60°$. The mosaicity was 0.968(2)°. A total of 804 frames were collected by using ϕ and ω scans with κ offsets, 17 s exposure time, a rotation angle of 0.7° per frame, and a crystal–detector distance of 38.6 mm. The space group was uniquely determined by the systematic absences. Equivalent reflections were merged. The data collection and refinement parameters are given in *Table 2*. A view of the molecule is shown in *Fig. 1*. The structure was solved by direct methods with SIR92 [31], which revealed the positions of all non-H-atoms. The non-H-atoms were refined anisotropically. All of the H-atoms were placed in geometrically calculated positions and refined by using a riding model where each H-atom was assigned a fixed isotropic displacement parameter with a value equal to 1.2 U_{eq} of its parent atom. The refinement of the structure was carried out on F^2 by using full-matrix least-squares procedures, which minimized the function $\Sigma w(F_o^2 - F_c^2)^2$. The weighting scheme was based on counting statistics and included a factor to downweight the intense reflections. Plots of $\Sigma w(F_o^2 - F_c^2)^2$ *vs.* F_c/F_c(max) and resolution showed no unusual trends. A correction for secondary extinction was applied. Refinement of the absolute structure parameter [32] yielded a value of −0.06(16), which confirms that the refined model corresponds with the true enantiomorph, although the precision of the determination is low.

4.3. *Determination of (−)-***11a**. The unit cell constants and an orientation matrix for data collection were obtained from a least-squares refinement of the setting angles of 11546 reflections in the range $4° < 2\theta < 55°$. The mosaicity was 1.016(3)°. A total of 322 frames were collected by using ϕ and ω scans with κ

Table 2. *Crystallographic Data of (−)-***10a** *and (−)-***11a**

	(−)-**10a**	(−)-**11a**
Crystallized from	pentane/Et_2O	pentane/Et_2O
Empirical formula	$C_{13}H_{17}FNO_3P$	$C_{13}H_{17}FNO_3P$
M_r	285.25	285.25
Crystal color, habit	colorless, prism	colorless, prism
Crystal dimensions [mm]	$0.12 \times 0.20 \times 0.32$	$0.17 \times 0.28 \times 0.40$
Temperature [K]	160(1)	160(1)
Crystal system	orthorhombic	triclinic
Space group	$P2_12_12_1$ (#19)	$P1$ (#1)
Z	4	1
Reflections for cell determination	48331	11546
2θ Range for cell determination [°]	4–60	4–55
Unit cell parameters:		
a [Å]	5.6609(2)	5.5530(2)
b [Å]	10.0766(4)	7.7169(4)
c [Å]	23.0798(8)	8.7115(4)
α [°]	90	104.506(2)
β [°]	90	91.269(3)
γ [°]	90	107.293(3)
V [Å^3]	1316.53(8)	343.18(3)
$F(000)$	600	150
D_x [g cm^{-3}]	1.439	1.380
$\mu(\mathrm{Mo}K_\alpha)$ [mm^{-1}]	0.224	0.215
Scan type	ϕ and ω	ϕ and ω
$2\theta_{(\max)}$ [°]	60	55
Transmission factors (min; max)	0.702; 0.974	0.873; 0.965
Total reflections measured	16761	8012
Symmetry independent reflections	3817	2854
R_{int}	0.105	0.046
Reflections with $I > 2\sigma(I)$	2715	2769
Reflections used in refinement	3817	2854
Parameters refined	173	172; 3
Final $R(F)$ ($I > 2\sigma(I)$ reflections)	0.0586	0.0442
$wR(F^2)$ (all data)	0.1503	0.1079
Weights	$w = [\sigma^2(F_o^2) + (0.073P)^2 + 0.4328P]^{-1}$ where $P = (F_o^2 + 2F_c^2)/3$	$w = [\sigma^2(F_o^2) + (0.0543P)^2 + 0.1646P]^{-1}$ where $P = (F_o^2 + 2F_c^2)/3$
Goodness of fit	1.034	1.096
Secondary extinction coefficient	0.018(3)	–
Final Δ_{max}/σ	0.001	0.001
$\Delta\rho$ (max; min) [e Å^{-3}]	0.45; −0.33	0.37; −0.24
$\sigma(d_{(C-C)})$ [Å]	0.003–0.005	0.003–0.004

offsets, 46 s exposure time, a rotation angle of 2.0° per frame, and a crystal–detector distance of 30.0 mm. The space group was determined from packing considerations, a statistical analysis of intensity distribution, and the successful solution and refinement of the structure. Equivalent reflections, other than *Friedel* pairs, were merged. The data collection and refinement parameters are given in *Table 2*. A view of the molecule is shown in *Fig. 2*. The structure was solved by direct methods with SIR92 [31], which revealed the positions of all non-H-atoms. The non-H-atoms were refined anisotropically. All of the H-atoms were placed in geometrically calculated positions and refined by using a riding model where

each H-atom was assigned a fixed isotropic displacement parameter with a value equal to $1.2U_{eq}$ of its parent atom. The refinement of the structure was carried out on F^2 by using full-matrix least-squares procedures, which minimized the function $\Sigma w(F_o^2 - F_c^2)^2$. The weighting scheme was based on counting statistics and included a factor to downweight the intense reflections. Plots of $\Sigma w(F_o^2 - F_c^2)^2$ *vs.* $F_c/F_c(\max)$ and resolution showed no unusual trends. A correction for secondary extinction was not applied. Refinement of the absolute structure parameter [32] yielded a value of $-0.07(10)$, which confidently confirms that the refined model corresponds with the true enantiomorph.

5. *Enzyme Kinetics*. 5.1. *General*. For the detailed experimental procedure and the methods of data analysis, see the preceding report [1]. The following parameters are as in [1]: Apparatus and general experimental conditions, phosphate buffer pH 7.00, AChE soln., ATC and DTNB solns., inhibitor solns., and the determination of K_m. P(O)F(O^iPr)$_2$ (diisopropyl fluorophosphate) was used as the standard reference.

5.2. Ellman *Assay* [14]. In a polystyrene cell (4 ml, $d = 1$ cm), phosphate buffer pH 7.00 (2 ml), DTNB soln. (100 µl), and ATC soln. (20 µl) were mixed and thermostatted at 25° (*ca.* 5 min). Then inhibitor soln. (x µl = 25, 20, 15, 10, and 5 µl; known [***I***]), and MeCN ((25 – x) µl) were added. At $t = 0$, the AChE soln. (1 ml) was added and the mixture gently mixed for 5 s. After 10 s, the monitoring of the absorption at 412 ± 2 nm (liberated bis-anion of 5-sulfanyl-2-nitrobenzoic acid) automatically started, and 900 data points were collected for 15 min at various concentrations of the inhibitor. As in the K_m determinations, the total volume was 3.15 µl, the concentration of the substrate [***S***] was 500 µM. Since all of the compounds were weak inhibitors, relatively high [***I***] were necessary, and due to solubility reasons, [***I***] < 300 µM had to be maintained. Per inhibitor, at least five measurements with different inhibitor concentrations were performed.

5.3. *Data Analysis*. a) *Irreversible Inhibitors* [15]. The integrated rate equation describing product generation (monitored by the absorbance A at λ 412 ± 2 nm) and the apparent rate constants (k_{obs}) is given by *Eqn. 1*. It is fitted ($R > 0.999$) to progress curves recorded at fixed [***S***] and variable [***I***] (primary plot, $A = f(t)$) to obtain a series of k_{obs} values and their standard errors (SE). The inhibition parameters are obtained from the secondary plots ($k_{obs} = f([\boldsymbol{I}])$) that result from weighted (SE^{-2}) linear or nonlinear regression according to *Eqns. 2* or *3*. The analysis of these plots enables a differentiation between the inhibition mechanisms: k_{obs} depends linearly upon the inhibitor concentration for mechanism *a* and hyperbolically for mechanism *b* (see *Scheme 5*). For mechanism *a*, the k_a values are calculated according to *Eqn. 2*, its slope $k_{obs}/[\boldsymbol{I}]$ is obtained from the linear regression (*Scheme 5*,*a*). The decisive plot for mechanism *b* is doubly reciprocal ($1/k_{obs} = f(1/[\boldsymbol{I}])$, *Eqn. 3*) and the K_D and k_p values are calculated by linear regression, the slope being $(K_D/k_p)(1 + [\boldsymbol{S}]/K_m)$ and the intercept $1/k_p$. The overall inhibitory potency (k_i) is expressed by k_p/K_D (see *Scheme 5*,*b*).

$$A = \frac{v_z}{k_{obs}}(1 - e^{-k_{obs} \cdot t}) \tag{1}$$

$$k_a = \left(\frac{k_{obs}}{[I]}\right)\left(1 + \frac{[S]}{K_m}\right) \tag{2}$$

$$\frac{1}{k_{obs}} = \left(\frac{K_D}{k_p}\right)\left(1 + \frac{[S]}{K_m}\right)\left(\frac{1}{[I]}\right) + \frac{1}{k_p} \tag{3}$$[18])

b) *Reversible Inhibitors* [16]. Since all the compounds were weak inhibitors, a clear differentiation of the primary plot type was not always straightforward. In particular, in some cases, the curvature of the primary plot ($A = f(t)$) was not too pronounced and rather converged towards a straight line as is characteristic for reversible inhibitors. When reversible behavior was assumed, the assays were performed each at five different inhibitor ([***I***]) and substrate concentrations ([***S***]) resulting in 25 data points per inhibitor. The inhibition parameters were evaluated from the secondary plots that were obtained by linearization methods according to *Lineweaver–Burk* ($1/k_{obs} = f(1/[\boldsymbol{S}])$) [16], *Hanes–Woolf*

[18]) The last term in *Eqn. 3* was erroneously printed as a subtrahend in [1].

($[\boldsymbol{S}]/k_{obs} = f([\boldsymbol{S}])$) [16], *Dixon* ($1/k_{obs} = f([\boldsymbol{I}])$) [16], and *Chan* ($1 + [\boldsymbol{S}]/K_m)(v_0 - v_i)/v_i[\boldsymbol{I}] = f([\boldsymbol{S}]/K_m)$) [17]. Comparative analysis of the individual results [2] lead to the differentiation of the various reversible inhibition mechanisms (competitive, noncompetitive, uncompetitive, linear mixed type) [16][17] (see *Scheme 5*, *c*).

5.4. *Results* (*Table 1*). The secondary plot ($k_{obs} = f([\boldsymbol{I}])$) exhibited a linear dependence for (±)-**10a**, (+)-**10a**, and P(O)F(^{i}Pr)$_2$. Hence, mechanism *a* was assigned. In the case of (+)- and (−)-**10b**, (−)-**11a**, and (+)- and (−)-**11b**, the secondary plot depended hyperbolically upon $[\boldsymbol{I}]$, and mechanism *b* was assigned for these compounds. Since the primary plots ($A = f(t)$) for (−)-**10a** and (+)-**11a** clearly displayed a linear dependence, these compounds are reversible inhibitors of AChE. According to the comparison of the different linearization methods [2], the linear mixed inhibition mechanism *c* could be assigned [16] (*Scheme 5*). However, the results of the linearization processes were ambiguous to some extent as exemplified for (+)-**11a**: Data evaluation according to *Lineveaver–Burk* suggested a linear mixed inhibition mechanism (intersection above the abscissa; from the intercepts (Δx, Δy) the modifying factors α and α' were calculated ($\alpha = -\alpha'/\Delta x K_m$, $\alpha' = v_{max}\Delta y$, and $K_I = [\boldsymbol{I}]/(\alpha - 1)$, $K'_I = [\boldsymbol{I}]/(\alpha' - 1)$) [16]: $K_I = 947$ μM, $K'_I = 7050$ μM ($\alpha = 7.44$) [2]. A similar result was obtained from the approach according to *Chan* ($K_I = 1/\Delta y$, slope $= 1/\alpha K_I$, $K'_I = \alpha K_I$) [17]: $K_I = 919$ μM, $K'_I = 8100$ μM ($\alpha = 8.81$) [2]. The value in *Table 1* is the rounded mean of these two approaches. The interpretation of the *Hanes–Woolf* diagram [16] resulted in a borderline case between noncompetitive and linear mixed inhibition (intersection just above the abscissa) [2]. Linearization according to *Dixon* [16] was ambiguous, too: The parallel straight lines are indicative for competititve inhibition, while others suggest a linear mixed mechanism [2]. Moreover, the rather close similarity of K_I and K'_I of (−)-**10a** may suggest a noncompetitive mechanism for this compound.

REFERENCES

[1] P. Lorenzetto, M. Wächter, P. Rüedi, *Helv. Chim. Acta* **2011**, *94*, 746.
[2] C. Clerc, 'Synthese und Charakterisierung von enantiomerenreinen N-heterocyclischen Phosphadecalinen als Inhibitoren von Acetylcholinesterase', Ph.D. Thesis, University of Zurich, 2008.
[3] S. Furegati, W. Ganci, F. Gorla, U. Ringeisen, P. Rüedi, *Helv. Chim. Acta* **2004**, *87*, 2629.
[4] S. Furegati, F. Gorla, A. Linden, P. Rüedi, *Chem.-Biol. Interact.* **2005**, *157–158*, 415.
[5] W. Ganci, E. J. M. Meier, F. A. Merckling, G. Przibille, U. Ringeisen, P. Rüedi, *Helv. Chim. Acta* **1997**, *80*, 421; S. Furegati, W. Ganci, G. Przibille, P. Rüedi, *Helv. Chim. Acta* **1998**, *81*, 1127.
[6] M. J. Stöckli, P. Rüedi, *Helv. Chim. Acta* **2001**, *84*, 106; M. J. Stöckli, P. Rüedi, *Helv. Chim. Acta* **2007**, *90*, 2058.
[7] S. Furegati, O. Zerbe, P. Rüedi, *Chem.-Biol. Interact.* **2005**, *157–158*, 418.
[8] C. Clerc, I. Matarazzo, P. Rüedi, *Helv. Chim. Acta* **2009**, *92*, 14.
[9] J. A. Dale, D. L. Dull, H. S. Mosher, *J. Org. Chem.* **1969**, *34*, 2543; G. R. Sullivan, J. A. Dale, H. S. Mosher, *J. Org. Chem.* **1973**, *38*, 2143; J. A. Dale, H. S. Mosher, *J. Am. Chem. Soc.* **1973**, *95*, 512; I. Ohtani, T. Kusumi, Y. Kahman, H. Kakisawa, *J. Am. Chem. Soc.* **1991**, *113*, 4092.
[10] M. Wächter, P. Rüedi, *Chem. Biodiversity* **2009**, *6*, 283.
[11] S. Furegati, M. Binder, A. Linden, P. Rüedi, *Helv. Chim. Acta* **2006**, *89*, 1351.
[12] M. Wächter, S. Jurt, A. Linden, P. Rüedi, in preparation.
[13] M. Wächter, 'Herstellung von optisch aktiven Organophosphaten mit *cis*- und *trans*-Decalingerüst zur Untersuchung der Inhibition von Acetylcholinesterase mittels Enzymkinetik und ^{31}P-NMR Spektroskopie', Ph.D. Thesis, University of Zurich, 2009.
[14] G. L. Ellman, K. D. Courtney, V. Andres Jr., R. M. Featherstone, *Biochem. Pharmacol.* **1961**, *7*, 88.
[15] A. Baici, *Biol. Chem.* **1998**, *379*, 1007.
[16] I. H. Segel, 'Enzyme Kinetics: Behavior and Analysis of Rapid Equilibrium and Steady-State Enzyme Systems', Wiley, New York, 1993; H. Bisswanger, 'Enzymkinetik, Theorie und Methoden', 3rd edn., VCH-Verlagsgesellschaft Weinheim, 2000.
[17] W. W. Chan, *Biochem. J.* **1993**, *311*, 981.
[18] A. Baici, P. Schenker, M. Wächter, P. Rüedi, *Chem. Biodiversity* **2009**, *6*, 261.

[19] M. Wächter, P. Rüedi, in preparation.
[20] C. J. Wilkins, *J. Chem. Soc.* **1951**, 2726.
[21] R. Hooft, KappaCCD Collect Software, Nonius BV, Delft, The Netherlands, 1999.
[22] Z. Otwinowski, W. Minor, 'Macromolecular Crystallography, Part A', in 'Methods in Enzymology', Vol. 276, Eds. C. W. Carter Jr., R. M. Sweet, Academic Press, New York, 1997, p. 307.
[23] R. H. Blessing, *Acta Crystallogr., Sect. A* **1995**, *51*, 33.
[24] E. N. Maslen, A. G. Fox, M. A. O'Keefe, in 'International Tables for Crystallography', Ed. A. J. C. Wilson, Kluwer Academic Publishers, Dordrecht, 1992, Vol. C, Table 6.1.1.1, p. 477.
[25] R. F. Stewart, E. R. Davidson, W. T. Simpson, *J. Chem. Phys.* **1965**, *42*, 3175.
[26] J. A. Ibers, W. C. Hamilton, *Acta Crystallogr.* **1964**, *17*, 781.
[27] D. C. Creagh, W. J. McAuley, in 'International Tables for Crystallography', Ed. A. J. C. Wilson, Kluwer Academic Publishers, Dordrecht, 1992, Vol. C, Table 4.2.6.8, p. 219.
[28] D. C. Creagh, J. H. Hubbell, in 'International Tables for Crystallography', Ed. A. J. C. Wilson, Kluwer Academic Publishers, Dordrecht, 1992, Vol. C, Table 4.2.4.3, p. 200.
[29] G. M. Sheldrick, 'SHELXL97, Program for the Refinement of Crystal Structures', University of Göttingen, Germany, 1997.
[30] C. K. Johnson, 'ORTEPII', Report ORNL-5138, Oak Ridge National Laboratory, Oak Ridge, Tennessee, 1976.
[31] A. Altomare, G. Cascarano, C. Giacovazzo, A. Guagliardi, M. C. Burla, G. Polidori, M. Camalli, SIR92, *J. Appl. Crystallogr.* **1994**, *27*, 435.
[32] H. D. Flack, G. Bernardinelli, *Acta Crystallogr., Sect. A* **1999**, *55*, 908; H. D. Flack, G. Bernardinelli, *J. Appl. Crystallogr.* **2000**, *33*, 1143.

Received September 20, 2011